View Article Online
View Journal

Green Chemistry

Cutting-edge research for a greener sustainable future

Accepted Manuscript

This article can be cited before page numbers have been issued, to do this please use: M. Noman, D. T. Awugichew, G. Yu and T. A. Bakare, *Green Chem.*, 2025, DOI: 10.1039/D5GC04029A.

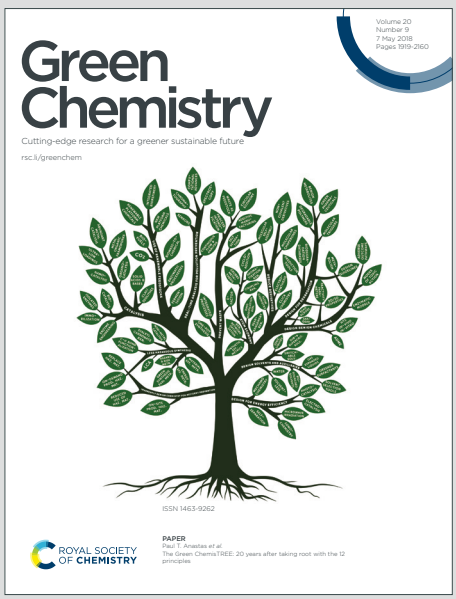

View Article Online
DOI: 10.1039/D5GC04029A

Green foundation

1. This study explores a green and efficient waste reuse by converting hazardous steel converter slag (120 million tons/year in China) and biogas residue into a functional nano-composite, preventing landfill and heavy metal leaching, and offering a low-cost green, recyclable, and stable alternative.

2. One-pot co-pyrolysis of renewable feedstocks, like carbon-rich biogas residue (waste prevention) with steel converter slag (Atom-economy), was performed at an energy-efficient temperature (700℃) under N_2 atmosphere, avoiding toxic solvents. This novel catalyst successfully eliminated the toxic pharmaceuticals in swine urine by synergistically enhancing ozonation via adsorption without toxic outputs, as an economical option for small pig farm urine treatment, confirmed by life cycle assessment.

3. Future direction may involve exploring the real potential of industrial and agricultural hazardous wastes for low-cost, green catalysts for environmental implications, life cycle analysis, and policy advocacy.

View Article Online
DOI: 10.1039/D5GC04029A

A greener strategy for ultra-fast adsorption promoted ozonation of livestock-excreted pharmaceuticals by co-pyrolysis of steel converter slag and biogas residue: Synergistic effects, environmental impacts and DFT study

Muhammad Noman [a, b], Dinkayehu Tsegaye Awugichew [a, b], Guangwei Yu* [a], Tekuma Abdisa Bakare[a, b]

[a] State Key Laboratory of Advanced Environmental Technology, Institute of Urban Environment, Chinese Academy of Sciences, Xiamen, Fujian 361021, China

[b] University of Chinese Academy of Sciences, Beijing 100049, China

* Corresponding author.

E-mail address: gwyu@iue.ac.cn (Guangwei Yu)

View Article Online
DOI: 10.1039/D5GC04029A

Abstract

China is the biggest pork-producing country, consequently raising serious environmental threats, due to the direct irrigation of untreated swine urine containing emerging toxic antibiotic residues like Ofloxacin. Similarly, China's steel and biogas industries generate steel converter slag residue (SCS) (120 million tons annually) and biogas residue (BR). SCS and BR's dumping or pilling is not eco-friendly due to the potential risk of leaching of heavy metals and eutrophication. Herein, the eco-friendly, one-pot co-pyrolysis of BR and SCS successfully achieved synergistic integration at various temperatures under a N_2 atmosphere, as confirmed by characterizations. Adsorption-promoted ultra-fast ozonation over Fe-SCS@BR-700℃ catalyst has eliminated OFL (20 mg/L), and swine urine's toxic organic pollutants. High-Performance Liquid Chromatography (HPLC) and Triple Quadrupole Liquid Chromatography-Mass Spectrometry (QTRAP ABI-3200) were employed successfully to trace and remove (<0.01 ppm) more than 16 toxic pharmaceuticals. ICP-MS and toxicity assessment revealed 0.2 g as a safer dosage. Wheat grains and Escherichia coli growth were seen in ozonated urine. Density functional theory, and Electron paramagnetic resonance revealed abundant active sites, exponential electron transfer, ROS generation like hydroxyl radicals ($^{\bullet}OH$), superoxide ($O_2^{\bullet-}$), and singlet oxygen ($^1O_2$) via ozone decomposition. Magnetization without regeneration gives robust recovery and recyclability. Fe-SCS@BR-700℃ reduces emissions, resource use, and costs more effectively comparatively. This study successfully established a greener, economical, and efficient heterogeneous catalyst to eliminate toxic pollutants from real swine urine at a small pigsty for safer urine resource irrigation, demonstrating a sustainable approach to treating waste by waste.

Keywords: Biogas residue, Steel converter slag, Ofloxacin, swine urine, Ultra-fast ozonation

View Article Online
DOI: 10.1039/D5GC04029A

Green foundation

1. This study explores a green and efficient waste reuse by converting hazardous steel converter slag (120 million tons/year in China) and biogas residue into a functional nano-composite, preventing landfill and heavy metal leaching, and offering a low-cost green, recyclable, and stable alternative.

2. One-pot co-pyrolysis of renewable feedstocks, like carbon-rich biogas residue (waste prevention) with steel converter slag (Atom-economy), was performed at an energy-efficient temperature (700°C) under N_2 atmosphere, avoiding toxic solvents. This novel catalyst successfully eliminated the toxic pharmaceuticals in swine urine by synergistically enhancing ozonation via adsorption without toxic outputs, as an economical option for small pig farm urine treatment, confirmed by life cycle assessment.

3. Future direction may involve exploring the real potential of industrial and agricultural hazardous wastes for low-cost, green catalysts for environmental implications, life cycle analysis, and policy advocacy.

View Article Online
DOI: 10.1039/D5GC04029A

1. Introduction

China is the world's largest pork producer, with nearly 50% of intensive pig farming. It utilizes 30% of antibiotics like Ofloxacin (OFL), causing environmental threats by massive untreated pig excrement irrigation (5.4 kg of urine per pig/day) [1, 2] . By 2030, antibiotic use could reach 107,472 tons per year [3]. Globally, developing regions traditionally use untreated pig urine mixed with manure for irrigation, as fertilizer, posing a risk to humans and ecosystems, causing antibiotic resistance genes (ARGs) to spread. Unfortunately, pig farms in Jizhou district, Hebei province, were identified as the primary contributors to antibiotic pollution in local water reservoirs, with a heightened risk to children's health, indicating an urgent need for enhanced pig urine wastewater treatment and regulatory measures [4]. Ofloxacin (OFL) is a commonly used antibiotic with broad-spectrum antibacterial properties. It enters the environment through urine, posing risks to drug-resistant bacteria, disrupting biological metabolism, in the aquatic environment. OFL was the most commonly detected in Jiaozhou Bay on the eastern coast of China [5]. Furthermore, due to the presence of 70% of small pigsties in China, OFL was also detected near rivers at 31.7 μg/L. OFL removal technologies like chlorination [6], coagulation [7], and electrochemical methods [8] involve a high complexity, slow, and energy-intensive process [9]. Notably, OFL behavior in the urine environment remains unexplored. For real swine urine's treatment by biological [10], anaerobic digester [11], and membrane treatment [12] methods is often slow, ineffective, and costly. While photocatalytic degradation [13] and the electrochemical method [11] are light-dependent and energy-intensive, especially for small pigsties. To date, high cost and low efficiency have been observed for real swine urine implication. Overall, small farms are lacking basic infrastructure or relying on costly, outdated, and low-efficiency systems [14]. Hence, low-cost and eco-friendly

View Article Online
DOI: 10.1039/D5GC04029A

technologies are urgently needed for safer swine urine resource utilization at small pigsties.

Due to rapid industrial development, biogas and steel industries generate a huge volume of hazardous solid wastes like steel converter slag (SCS) and biogas residue (BR). China, as the largest steel producer, only recycles 35% of the SCS out of 120 million tons annually; the rest is dumped into the open environment [15]. BR contains foul odor, pathogenic microorganisms (polychlorinated biphenyls, chlorinated paraffin), and is utilized as fertilizer or landfill material. Both can leach heavy metals into soil and water [16 17]. Further, despite a limited waste management system, the World Bank estimated global waste generation could surpass 3.40 billion tons by 2050 [18]. Therefore, novel, greener, and advanced approaches, such as converting BR and SCS into green nano-composites for practical environmental remediation, are crucial.

To address the hazardous wastes, for environmental concerns, traditional complex and high-cost catalyst synthesis is gradually shifting towards low-cost, non-toxic outputs. Various agricultural, industrial, and municipal wastes are being repurposed for waste-based catalysts through innovative scientific methods [19]. Current strategies, efforts to recover useful substances from industrial slags, by alkali dissolution-acid precipitation, washing, and recrystallization[20]. Such approaches are costly, water-intensive, and yield low outputs, while also causing secondary pollution, thus affecting sustainability and efficiency. Interestingly, advanced oxidizing processes (AOPs), like persulfate (PS) activation [21], photocatalytic [22], and Fenton-like oxidation [23], utilized the solid waste-carbonaceous catalysts (SW-CCs), for various environmental remediations due to reactive oxygen species (ROS) like hydroxyl radicals ($^{\bullet}OH$), oxygen radicals ($O_2^{\bullet-}$), and singlet oxygen ($^1O_2$) [24]. However, metal and non-metal synergy has yet to be elucidated. Given the coexistence of organic substances in BR and

View Article Online
DOI: 10.1039/D5GC04029A

metals like Fe in SCS, it could be an attractive prospect for in situ hazardous industrial residues upcycling, for efficient nano-composites utilization for AOPs. This could be a pioneer of exogenous-free nano-composites from dual industrial residue streams, leveraging the inherent organic substances and metals as precursors. Fortunately, eco-friendly and low-cost, one-pot co-pyrolysis of SCS (Fe-rich) and BR (C-source) can be innovative to activate the ozone (O_3) combined with adsorption, for enhanced ROS to degrade real swine urine's organic pollutants. SCS not only enhanced the active sites, graphitization, reusability, and conductivity of BR but also made it an adsorbent, ion exchanger, due to Fe_2O_3, Fe_3O_4, and FeO (Fe^{+2}, Fe^{+3}, and Fe^0) [25, 26]. Thus, this strategy significantly enhances the utilization of all components of residues with potential synergistic effects, and can be expected to achieve sustainable utilization of low-cost industrial residues. Nevertheless, to the best of our knowledge, firstly, this green strategy by catalyst (Fe-SCS@BR) for adsorption-assisted ultra-efficient catalytic ozonation degradation of various toxic antibiotics in real swine urine was developed, supporting the novel concept of "treating waste with waste."

Herein, we proposed, for the first time, a heterogeneous catalyst (Fe-SCS@BR) for the elimination of combined antibiotics from manure separated swine urine, and OFL under stimulated urine by only using industrial waste residues as raw materials, by a proposed fixed-bed adsorption-promoted ozonation reactor under environmentally realistic conditions. Notably, enhanced combined degradation of various toxic emerging antibiotics like Sulfamethoxazole, Sulfamethazine, Sulfamonomethoxine, Quinolone Antibiotics (Fleroxacin, Ofloxacin, Norfloxacin), and Antiparasitic Drugs (Levamisole) was observed from real swine urine. Characterizations proved enhanced Fe-ions dispersion, electron transfer ability, active sites, and reusability. Fe-SCS@BR-700℃ showed

View Article Online
DOI: 10.1039/D5GC04029A

optimum ROS for degradation, COD, and TOC removal of OFL and toxic pharmaceuticals of real swine urine. Density functional theory (DFT) confirmed indirect O_3 adsorption and ROS affinity. Mechanism and ICP-MS toxicity revealed a major role of $O_2^{\bullet-}$ and successful wheat and E. coli growth. This study contributes to novel and cost-effective implications for a greener environment.

2. Materials and methods

2.1 Materials and chemicals

All information related can be found in the **Text. S1.**

2.2 Sampling and solution preparation

Raw BR was collected by Xiamen Eastern Solid Waste Treatment Center, which was generated by livestock manure. While raw SCS was collected from the Anhui province steel industry. The chemical composition and properties of SCS and BR are shown in the **Table. S1**. Additionally, by utilizing the urine-manure separation method, real swine urine was collected from the treatment system (500 m^3/d). Swine urine samples were collected in October (for initial experiments) and December (AOPs experiments) 2024, from Xinxing County pig farm, Yunfu City, Guangdong Province, China. For a lab-scale pilot study, fresh swine urine (5 L) samples were collected in an acid-washed polyethylene bottle from a facility located on-site, including primary clarifier, anaerobic fermentation, secondary clarifier, sedimentation, and chlorination disinfection. Notably, this system could not significantly degrade swine urine's organic matter and antibiotics. Additionally, at the lab scale, by following standards, stimulated urine and super deionized (SDI) water solutions were also prepared, having

View Article Online
DOI: 10.1039/D5GC04029A

Ofloxacin (OFL) (20mg/L). All solutions' characteristics are mentioned in the **Text. S2** and **Figure S8**.

2.3 Synthesis of Fe-SCS@BR catalyst

As a pretreatment process, 5 g of raw SCS was rubbed and shaken three times alternately into super deionized water (SDI) (1000 ml) for 24 hr. and washed with ethanol to remove its dust and impurities. Afterward, cleaned raw SCS was placed into the oven at 105℃ until dry. Then, it was ground into a fine powder by ball milling until 100 mesh. Moreover, 25 g of raw BR was cleaned and ground to 100 mesh. Ecological one-step, co-pyrolysis of uniformly mixed BR and SCS with a ratio of 5:1 was done at 300℃, 500℃, and 700℃ until 45 min under N_2 atmosphere separately (**Table S1** and **Figure S7).** Finally, all prepared catalysts were finely ground separately and labeled as Fe-SCS@BR 300℃, Fe-SCS@BR 500℃, and Fe-SCS@BR 700℃, as illustrated in **Figure 1 (a).**

2.4 Catalytic Characterization

The physiological morphology and elemental composition of all catalysts were examined using advanced technologies, including Energy Dispersive Spectroscopy (EDS), Scanning Electron Microscopy (SEM), Transmission Electron Microscopy (TEM), Vibratory sample magnetometry (VSM), and X-ray photoelectron spectroscopy (XPS). All information related to characterization can be found in the **Text. S3**.

2.5 Experimental procedure for adsorption-promoted catalytic ozonation degradation

All experiments were conducted in a 250 mL beaker at 25℃ ± 0.5℃. Using standard procedure, stimulated urine containing OFL (20 mg/L) was prepared, having low-concentration Ammonium bicarbonate (NH_4HCO_3) (0.20 mole/L) [27]**(Text S2, Figure S8).** SDI solution of OFL was prepared

View Article Online
DOI: 10.1039/D5GC04029A

with similar concentrations for comparison. Finally, stimulated urine and SDI solutions were stored at 4℃ in a refrigerator. Each 200 mL of solution had 0.20g (1:1000) of catalyst with continuous adsorption (650 rpm) using a magnetic stirrer, and O_3 flow of 5.50 ± 0.5 mg/L at 25℃ ± 0.5℃, while the initial pH was kept unchanged till 9.17 to meet real conditions. Samples were collected at a specific time and filtered into a conical centrifuge tube of 1.5 mL using a 0.45-μm polyether sulfone syringe, separately.

2.6 Adsorption-promoted lab-scale fixed-bed reactor for swine urine treatment – A pilot study

A lab-scale pilot study was adopted to reveal the optimum catalyst SCS@BR-700℃'s potential for a real environmental implication. Firstly, fresh swine urine was pre-treated by vacuum filtration, filled in a liquid phase vial, and a solid phase extraction was done to remove suspended solids. Secondly, nitrogen blowing was performed to remove volatile organic compounds. Swine urine samples were diluted using methanol, and a standard method for sample preparation was utilized. Finally, adsorption-supported catalytic ozonation degradation experiments were performed in a fixed-bed reactor (5L) **(Figure S7b, Figure 3h)**. All samples were collected and filtered at a certain time. To detect the swine urine's toxic pharmaceutical intensities before and after reaction, QTRAP ABI-3200 mass spectrometry was employed. Further procedure details are mentioned in **Text S4.**

2.7 Analytical methods

OFL concentrations after the reaction were determined using HPLC (Agilent 1200) equipped with a C18 column (50 mm x 4.6 mm x 5 μm). Further, a UV-Vis spectrophotometer was also employed to measure OFL concentration at specified absorption wavelengths (nm). Triple Quadrupole Liquid Chromatography-Mass Spectrometry (QTRAP ABI-3200) was employed for real swine urine

View Article Online
DOI: 10.1039/D5GC04029A

toxic pharmaceuticals' intensities detection, while HPLC (Agilent 1200) was employed after swine urine catalytic ozonation to measure degraded pharmaceutical concentrations (mg/L)**.** Total organic carbon (TOC) and chemical oxygen demand (COD) are used for the measurement of biodegradable and non-biodegradable organic compounds. Suspended solids in the real swine urine were determined by the gravimetric method, and ammonia nitrogen (NH_3-N) contents were measured by the Nano reagent spectrophotometric method. Three-dimensional excitation-emission matrix fluorescence spectroscopy (3D-EEM) was used to measure the organic decomposition after reaction. Further, all details of the measurement methods are mentioned in **Text S5.**

3. Results and discussion

3.1 Characterization

Figure 1 (b-g) depicts the SEM images of raw BR, SCS, and pyrolyzed catalyst (Fe-SCS@BR) at different temperatures. Raw BR and SCS **(Figure 1a)** can be easily distinguished before and after co-pyrolysis. Comparatively, SCS **(Figure 1c)** shows irregular, compacted, and crystalline smooth surfaces. **Figure 1d** shows the mixture (SCS: BR) before pyrolysis, with irregular, rough, and grainy SCS's metal around the BR particles. **Figures 1e-g** show the Fe-SCS@BR at various temperatures, indicating the fused BR's loose and porous surface surrounded by SCS. Notably, at 300℃ to 700℃, the loose, non-compacted, and bright surfaces were more visible.

View Article Online
DOI: 10.1039/D5GC04029A

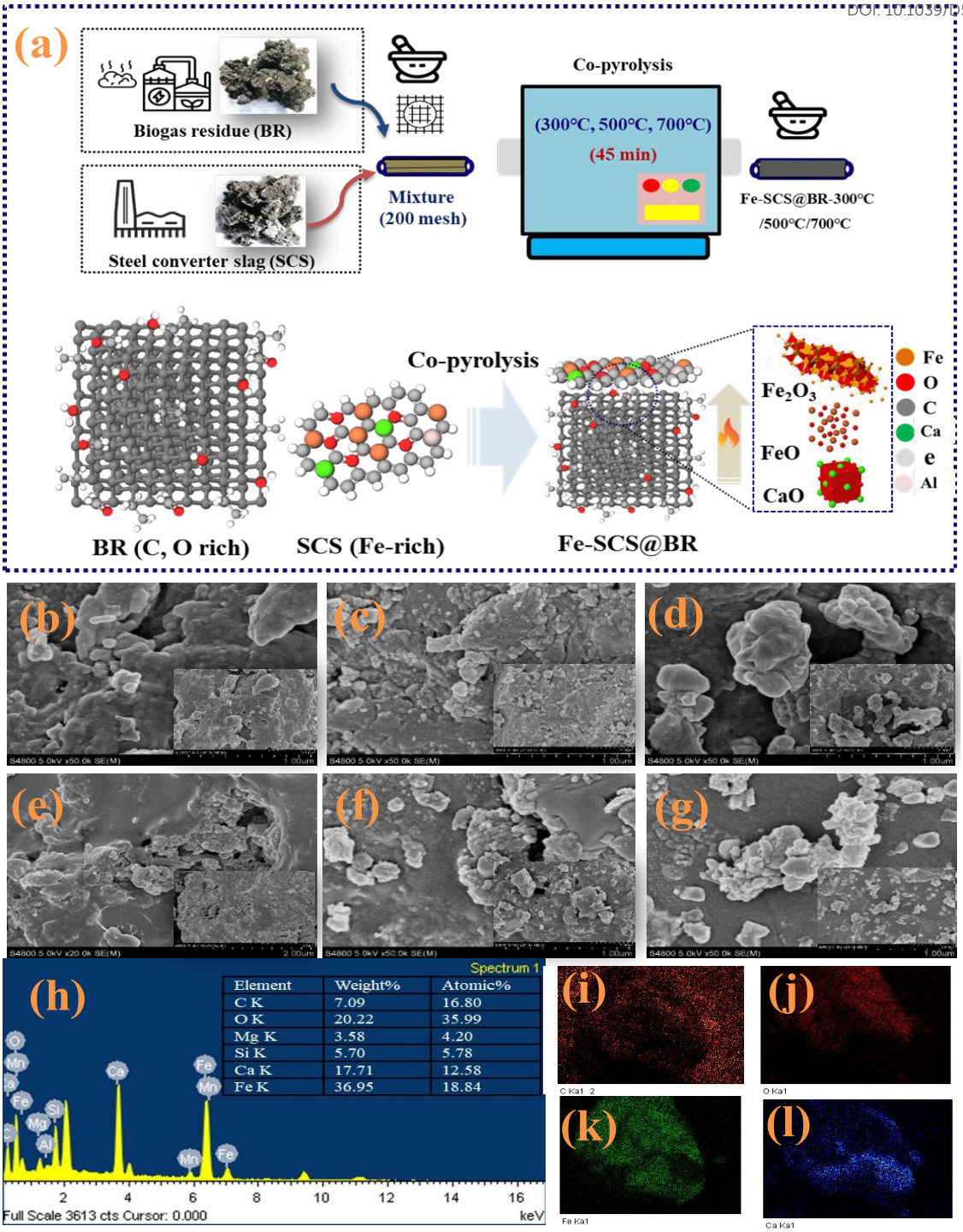

Figure 1:(a) Schematic synthesis (b) BR (Biogas residue) (c) Steel converter slag (SCS) (d) Raw mixture (SCS: BR) (1:5) (e) Fe-SCS@BR 300℃ (f) Fe-SCS@BR 500℃ (g) Fe-SCS@BR 700℃ and (h) EDS of Fe-SCS@BR 700℃, (i) C g (j) O g (k) Fe g (l) Ca g

Fe-SCS@BR 700℃'s EDS **(Figure 1h)** confirms the significant contents of C, O, Ca, Al, Si, and Fe, due to successful dispersion by co-pyrolysis. It confirms that SCS's metal content's uniform

View Article Online
DOI: 10.1039/D5GC04029A

distribution could enhance the ozone decomposition. Hence, higher temperature could enhance metal active sites, and better synergy **(Figure S1 l-n)**. **Figure 2a** shows the XRD results of all raw and pyrolyzed catalysts. It was seen that (Fe_2O_3), (32-36˚), magnetite (Fe_3O_4), (44.86˚) peaks were shifted after pyrolysis, Fe_2O_3 (hematite) (2θ = 37.97˚, 29.71˚), Fe^0 (43.27˚-48.74˚), SiO_2 (2θ = 50.11˚, 39.54˚, 26.65), calcite (28.15˚-32.02˚), $CaCO_3$ (2θ = 36.54˚, 29.30˚), and Quartz III (39.52˚) crystalline peaks were also successfully revealed. Notably, Fe^0 distinct peaks were seen at higher temperatures in favor of O_3 activation for ROS [28] **(Equations 1-2)**.

$$2Fe_2O_3 + 3C \rightarrow 4Fe^o + 3CO_2 \qquad (1)$$

$$Fe_2O_4 + 2C \rightarrow 2Fe^o + 2CO_2 \qquad (2)$$

Figure 2b shows FT-IR with all crucial functional groups in Fe-SCS@BR. Overall, Si-O stretching, $CaCO_3$, and Fe-O vibrations were observed at 1036.59 cm^{-1}, 872.18 cm^{-1}, and 563.13 cm^{-1}, respectively [29]. The pristine and raw mixture of SCS and BR shows C-C stretching (1512.46 cm^{-1}), while after co-pyrolysis, C=C stretching (1645.05 cm^{-1}) is more obvious comparatively. The disappearance of OH peaks (2929.9-2803.14 cm^{-1}) due to temperature rise, while Fe-O became more apparent. **Figure 2c** and **Table. S1** depicts the XPS analysis of non-pyrolyzed and pyrolyzed catalysts to explore elemental composition. Raw materials like BR and SCS had distinct C-1s, Ca-2p, and O-1s peaks, while the raw mixture showed combined peaks. Interestingly, after co-pyrolysis at 300℃, 500℃, and 700℃, the presence of Fe and Al was increased from 0.04% to 0.016% and 0.18% to 2.57%, respectively, while C, O, Ca, and Si showed some decline. Overall, the XPS results were consistent with XRD, FT-IR, and SEM.

To reveal the separation and reusability of the catalyst, VSM of Fe-SCS@BR (300℃, 500℃,

View Article Online
DOI: 10.1039/D5GC04029A

and 700°C) was performed **(Figure 2d)**. Hysteresis loops of the Fe-SCS@BR-300°C/500°C/700°C showed magnetic saturation value (Ms) of 0.13 emu/g, 3.944 emu/g, and 11.63 emu/g, while residual magnetization (Mr) was 0.44 emu/g, 0.85 emu/g, and 2.409 emu/g, respectively.

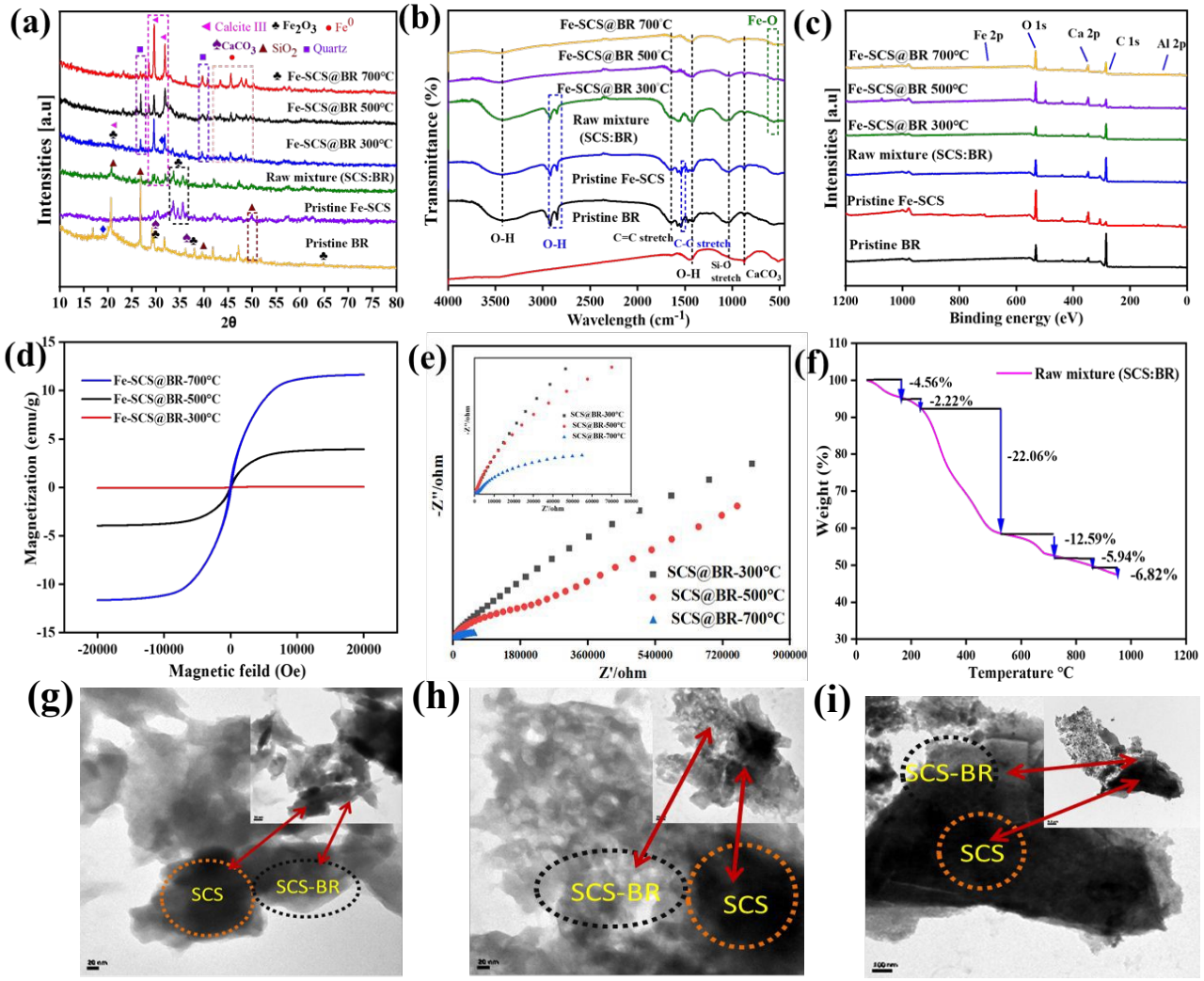

Figure 2: (a) XRD, (b) FT-IR (c) XPS of BR, SCS, Raw mixture (SCS: BR, Fe-SCS@BR (pyrolyzed) (d) VSM (e) EIS, (f) TGA of mixture (SCS: BR) (1:5), TEM of (g) Fe-SCS@BR-300 (h) Fe-SCS@BR-500 (i) Fe-SCS@BR-700°C

Notably, ferromagnetic property has been enhanced with temperature rise and high coercivity (Hc). **Table. S2** shows all catalyst Ms, Mr, Hc, and Mr/Ms VSM values. **Figure S10** depicts the catalysts 'contact angles, where hydrophilicity increases with co-pyrolysis temperature rise. **Figure S1**

View Article Online
DOI: 10.1039/D5GC04029A

b represents the catalyst's zeta potential. Enhanced co-pyrolysis could enhance the suspension or neutrality (pH_{pzc} of 4.3) of the catalytic surface in favor of pollutant adsorption.

Figure 2e and **Figure S1a** reveal the electrochemically enhanced properties of Fe-SCS@BR700℃, as measured by electrochemical impedance (EIS). Interestingly, with the co-pyrolysis temperature rise, the semicircle reduces, meaning the electron transfer ability increases or the charge transfer resistance decreases. **Figure S1a** depicts cyclic voltammetry CV curves of all catalysts, which are directly proportional to the co-pyrolysis temperature of all catalysts, showing a significant current response against specific potential scan rates. Based on observations, SCS@BR-700℃ has shown the highest electron transfer ability and current response. XPS results also confirm EIS and CV results, due to the iron content at higher temperatures **(Figure 2c).** To understand the optimum co-pyrolysis temperature, thermogravimetric (TG) curves of BR, SCS, and mixture (SCS: BR) under N_2 atmosphere were performed (**Figure S1 (c)**, **Figure 2(f))**. Raw BR's TG curve, at 146.5℃, showed a weight loss was 5.22%, but 30.75% at 381.9 ℃ in the second stage, due to BR's leftover constituents burning after anaerobic decomposition, like lignin, crystalline cellulose, and hemicellulose [30] (**Figure S1 (c))**. However, BR's most suitable co-pyrolysis temperature can be 535.5℃ (14.59%) to 946.8℃ (6.82%) due to maximum reduction in weight loss. **Figure 2 (f)** also indicates the least weight loss of the raw SCS (**Figure S1(c))**, which is 1.27% at 947.5℃, mainly due to the presence of heavy metals like Fe, Ca, Si, and Al. Notably, **Figure 2 (f)** depicts the combined weight loss of 4.56% at 158.93℃ and 2.22% at 222.71℃, but suddenly decreases to 22.06% at 526.43℃ due to BR's carbon contents, then stops at 12.56% at 716.95℃ due to SCS's metals. Hence, it was concluded that the mixture (SCS: BR) (1:5) could be maximally stable until the optimum temperature of 700 ℃.

View Article Online
DOI: 10.1039/D5GC04029A

TEM images, **Figure 1 (g-i),** show that light blackish color layers are due to overlapping SCS and BR at various temperatures [31]. Notably, temperatures rise, giving a more obvious overlapping of SCS and BR, indicating the optimum temperature. Finally, advanced characterization confirmed a strong synergistic effect between BR and SCS nanocomposites, elucidating the underlying mechanisms and demonstrating potential for real wastewater implications.

3.2. Catalytic Ozonation Degradation

3.2.1 Comparison of the catalytic performance for OFL

Firstly, the limited adsorption potential (14.54%) was revealed for stimulated urine containing OFL **(Figure S3)**. Hence, newly prepared novel catalysts were exposed to adsorption-enhanced catalytic ozonation degradation of stimulated urine over 100 minutes. **Figure 3 (a-b)** represents the comparative catalytic ozonation activities of all catalysts (Fe-SCS@BR-300℃/500℃/700℃) under SDI and stimulated urine containing OFL (20 mg/L) for comparison, respectively. **Figure 3 (a)** depicts that OFL (20 mg/L) was completely removed, in just 20 min, by catalysts prepared at enhanced temperature (i.e., 500℃, 700℃) under SDI solution. While **Figure 3(b)** shows that a similar concentration of OFL was removed 98 98% over 100 min under stimulated urine. This scavenging effect is due to the variety of urine's organic and inorganic constituents (i.e., urea, creatinine, salts, and organic acids) that can easily occupy the catalyst active sites and hinder the ROS generation. Based on observation, the Fe-SCS@B-700℃ catalyst was the best-performing optimum catalyst. Finally, it was concluded that enhanced co-pyrolysis temperature and medium matrix could play a key role in better synergy and pollutant degradation. For calculating the catalytic activity, certain information is given in the **Text. S4.**

View Article Online
DOI: 10.1039/D5GC04029A

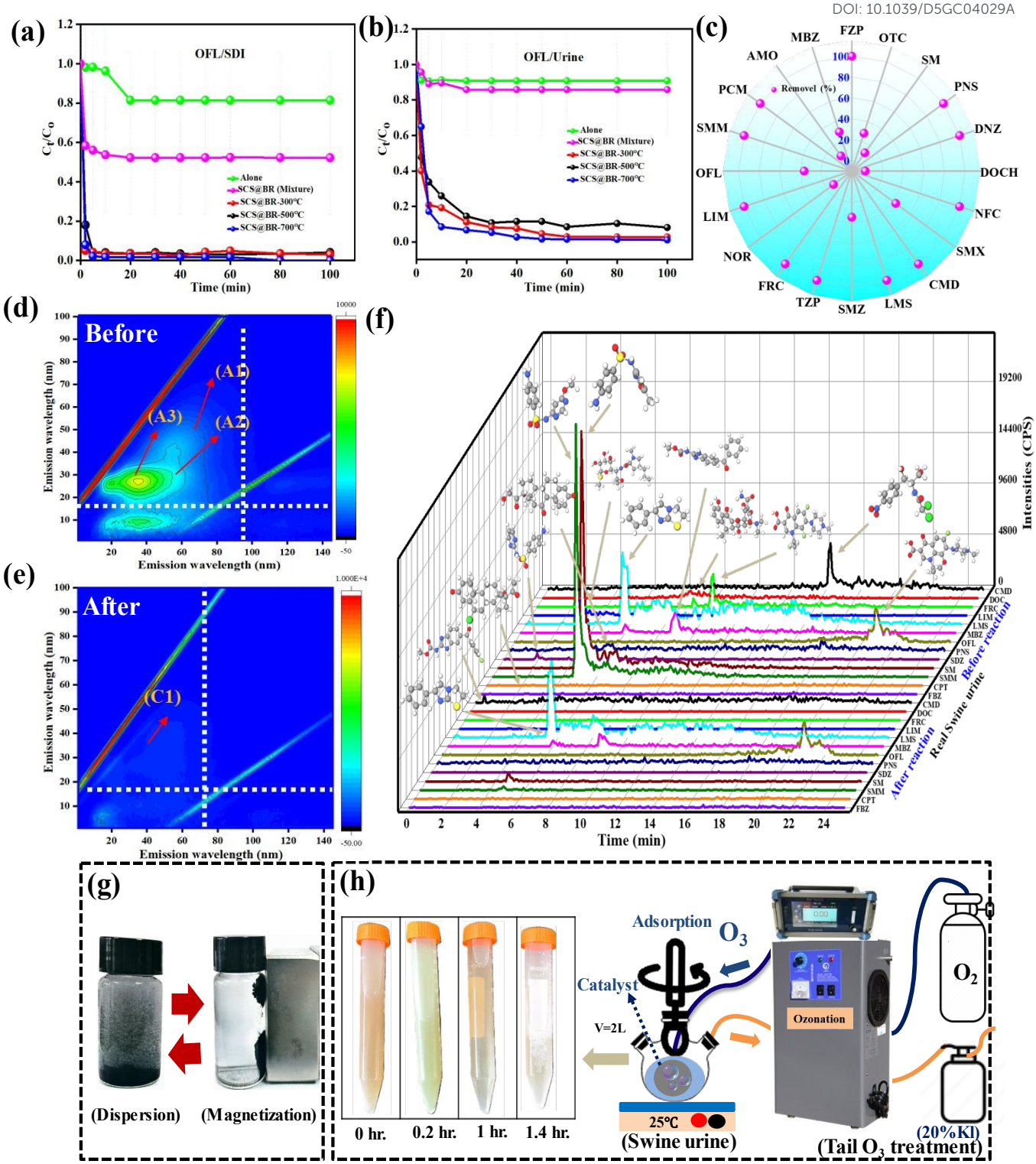

Figure 3: Catalytic activity over different catalysts (a) Ofloxacin (SDI water), (b) Ofloxacin (stimulated urine), removal efficiency of pharmaceuticals in (c) real swine urine, after reaction, (d-e) swine urine's 3D-EEM spectrum, before and after reaction. (f) Pharmaceutical intensities (cps) in real swine urine before and after reaction, over Fe-SCS@BR-700℃/O_3. **Conditions:** [OFL] = 20 mg/L,

$[O_3]$ = 5.5± 0.5 mg/L, [V] = 200 mL, catalyst = 0.20 g, pH (urine) = 8.85, pH (stimulated) = 9.17, T = 25℃ ± 0.5℃, Time = 100 min, revolutions = 650 rpm (g-h) Catalytic magnetization and lab scale plot study treatment for real swine urine. **Conditions**: [V] = 2 L, $[O_3]$ = 27.5± 0.5 mg/L, catalyst = 2 g, pH = 8.85, T =25℃ ± 0.5℃, Time = 100 min, revolutions = 1200 rpm.

Finally, Fe-SCS@B-700℃ was successfully tested for OFL degradation under the scavenging effects of stimulated urine (HCO_3^-/CO_3^{2-}, chloride (Cl^-), and ammonium (NH_4^+) until the third cycle (>75%) **(Figure S12a).** Further, a comprehensive study comparison based on removal efficiency confirmed its effectiveness **(Figure S13a, S14b, Table S11).**

3.2.2 Performance evaluation of the fixed bed reactor and environmental implications

Real swine wastewater challenges traditional treatments with its high levels of antibiotics, nutrients, and organics. While proposed adsorption-assisted catalytic ozonation enhances pollutant-oxidant contact and ozone breakdown, achieving efficient degradation in a single fixed bed reactor system **(Figure h), (Figure S7 b).** An optimum catalyst (Fe-SCS@BR-700℃) was utilized, over swine urine-manure separated adsorption-supported ozonation, over 100 min, with real environmental conditions, and samples were obtained. Firstly, QTRAP ABI-3200 was employed to investigate toxic swine urine's pharmaceutical pollutants **(Text S4), (Figure S11a-b** and **Table S7a-b).** To detect the intensities, the drug library's comparison helped to find the organic pollutants' molecular formulas and molecular weights extracted by a mass spectrometer. As per analysis, three sulfonamides (Sulfamethoxazole, Sulfamonomethoxine, Sulfamethazine), three Quinolone Antibiotics **(**Fleroxacin, Ofloxacin, Norfloxacin), four Antibiotics (Oxytetracycline, Levamisole, Lincomycin, Doxycycline), Antiparasitic Drugs (Mebendazole), Sedatives and Hypnotics: Flunitrazepam

View Article Online
DOI: 10.1039/D5GC04029A

(Rohypnol), Central Nervous System (CNS) Stimulants: (Donepezil), Steroidal Antiandrogens (Chlormadinone) and Corticosteroids (Prednisone) were successfully detected **(Figure 3f, Figure.S11a, Table.S7a)**. After the reaction, intensities of Sulfamethoxazole, Sulfamethazine, Sulfamonomethoxine, Oxytetracycline, Quinolone Antibiotics (Ofloxacin, Fleroxacin, Norfloxacin), and Antiparasitic Drugs (Levamisole) were not detected **(Figure 3f) (Figure S11b, Table S10 b).** Additionally, the HPLC standard curve method helped to determine each antibiotic concentration in swine urine **(Text S4)**. **Figure 3f** shows, the removal percentage of the highest intensified antibiotics after the reaction (<0.01 ppm) as follows SMX (42.70%) > OFL (36.29%) > SMZ (34.24%) > MBZ (29.36%)> OTC (28.07%)> SM (11.48 %) >AMO (7.93%) > NOR (7.93%), and DOC (3.044%), meeting China's national standard (GB/T 32951-2016) for organic fertilizer[32]. While LMS, PCM, NFE, LMS, SMZ, SM, SMM, MBZ, FZP, DNZ, and PNS were not detected. Finally, the used catalyst was separated by magnetization for further reusability without regeneration **(Figure 3g).**

Additionally, as secondary benefits, swine urine-manure mixed was also performed, where P (21%), Ca (18.8%), Na (13.2%), and K (9.8%) reduction was noticed via struvite crystallization and recovery by adsorption over Fe-SCS@BR-700℃/O_3, contributing to sustainable circular agriculture innovation [33] **(Figure S5a).** FTIR of ozonated swine manure's 35% reduction in C-H (2900 cm^{-1}) and 28% in amide I (1650 cm^{-1}) means enhancing biogas potential by lipid reduction, and reducing NH_3 toxicity risk by protein breakdown, respectively. Notably, new C=O (1700 cm^{-1}) and C-O (1200 cm^{-1}) peaks indicate an increase in biodegradable intermediates [34] (**Figure S5b)**. This green adsorption-catalytic ozonation process eliminates antibiotics and enables circular livestock waste management.

View Article Online
DOI: 10.1039/D5GC04029A

3.2.3 COD, TOC, and 3D-EEM of degraded OFL and real swine urine

To determine the optimum catalyst activity, Fe-SCS@BR-700 ℃, chemical oxygen demand (COD), Total organic carbon (TOC), and three-dimensional excitation-emission matrix (3D-EEM) fluorescence spectra were measured. **Figure S4 (a-b)** depicts significantly higher COD removal efficiency for OFL till 67.96% in SDI water as compared to stimulated urine, 20.66% due to scavenging impacts. **Figure S4c** depicts 71% COD removal for real swine urine effluents. **Figure 3c** depicts that TOC removal over Fe-SCS@BR-700℃/O_3 of real swine urine was higher, comparatively, due to a favorable composition for microbial activity [35]. Similarly, **Figure S4 (d-e)** showed that Fe-SCS@BR-500℃ has a higher removal than Fe-SCS@BR-300℃ in both solutions. After reaction, 3D-EEMs revealed that the real swine urine and OFL-stimulated urine's degraded organic ingredients [36]. **Figure.3(d-e)** depicts 3D-EMM spectra of real swine urine having complex organic substances (antibiotics, protein, humic matter, etc.) indicated by A1, A2, and A3 (Emission wavelength x = 20-80 nm, y = 2-60 nm) significantly transformed to less harmful and easily degradable compounds C1 after 100 minutes, respectively. **Figure S2 (a-b)** indicates OFL high fluorescence spectrum divided into E, F, and G, where organic pollutants were successfully degraded into H in a urine environment. Hence, it was observed that considerable organic matter was degraded successfully.

3.2.4 Factors Affecting Catalytic Ozonation Degradation

To optimize the experimental conditions, various factors like catalytic dose, ozone, pollutant concentration, initial temperature, and pH values were considered under stimulated urine containing OFL. **Figure 4 (a-f)** shows that the initial natural pH of the stimulated urine having OFL (9.70) removal efficiency was 91.81%. It is already documented that more alkaline conditions are more

View Article Online
DOI: 10.1039/D5GC04029A

favourable in catalytic ozonation [37]. Meanwhile, a more acidic environment could convert reactive species to weaker active species [27]. Notably, oxygen-reactive species like $^1O_2$ have a high pH tolerance, already confirmed by EPR **(Figure 6f)**, resulting in stable degradation of OFL in urine [38]. In **Figure 4 (b)** for pollutant loading, it can be seen that 20 mg/L (91.81%) was a more suitable dose. It is due to fewer intermediates, competition, and abundant active sites at a lower pollutant load [39].

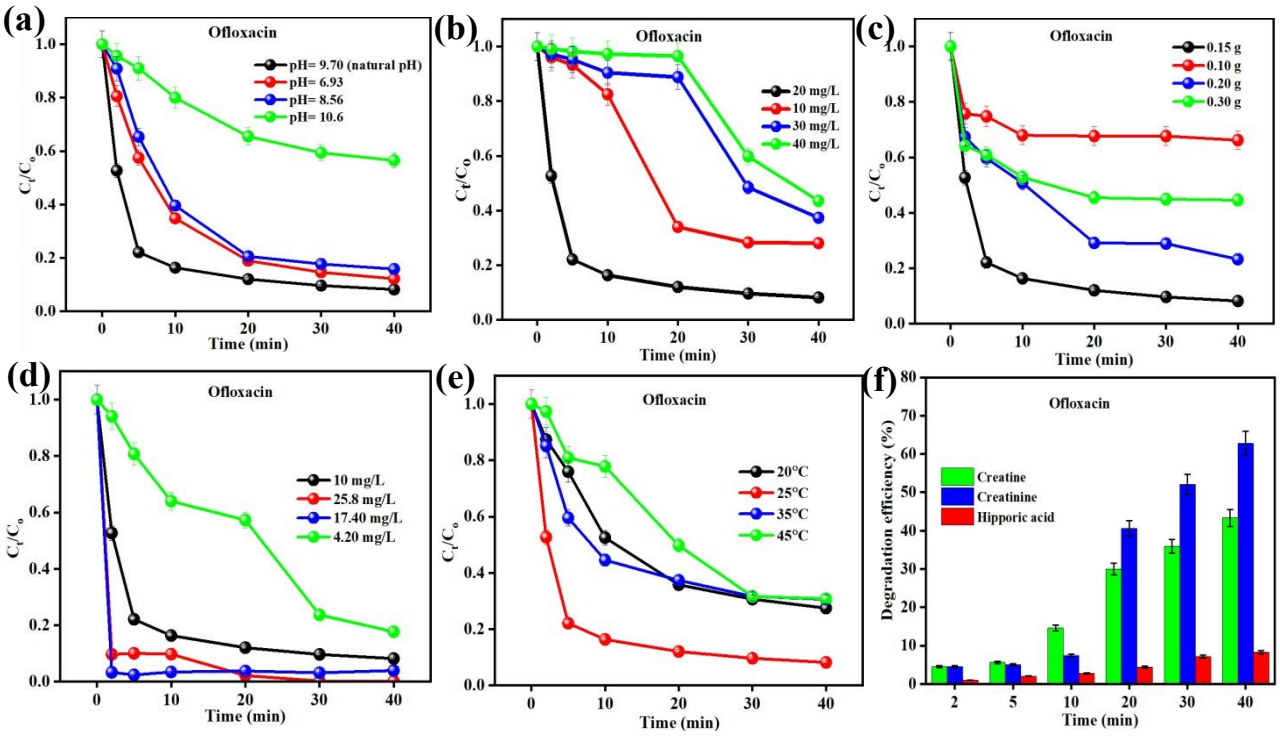

Figure 4: Ofloxacin degradation over stimulated urine under different (a) pH values, (b) pollutant load, (c) catalytic dosages, (d) different ozone concentrations over different temperatures over Fe-SCS@BR-700℃. (f) Effects of creatine, creatinine, and hippuric acid. **Conditions:** [V] = 200 mL, Time = 100 min, revolutions = 650 rpm, while [O_3], catalyst, pH, Temperature, [OFL] concentrations were kept changing.

Figure 4 (c) shows higher degradation at 0.15g, which is the optimum catalytic dosage**.** Based on the evaluation, **Figure 4 (d)**, it was seen that a 17.40 mg/L O_3 for OFL degradation is most efficient. This means that a higher O_3 dosage could increase the scavenging effects, thereby decreasing degradation [40]. While **Figure 4 (e)** shows the critical role of temperature in degradation under a urine

View Article Online
DOI: 10.1039/D5GC04029A

matrix, where at 25℃, enhanced catalytic temperature was observed. Notably, urine's creatine, creatinine, and hippuric acid can directly affect the degradation. These substances are endogenous, in urine, and significantly affect the degradation of pharmaceuticals and other organic pollutants. Therefore, considering stimulated urine, the effects of creatine, creatinine, and hippuric acid should be evaluated during the reaction. **Fig. 4f** depicts that these ingredients have overall negative impacts on antibiotic degradation in stimulated urine due to scavenger effects.

4. Identification of ROS and active sites assessment

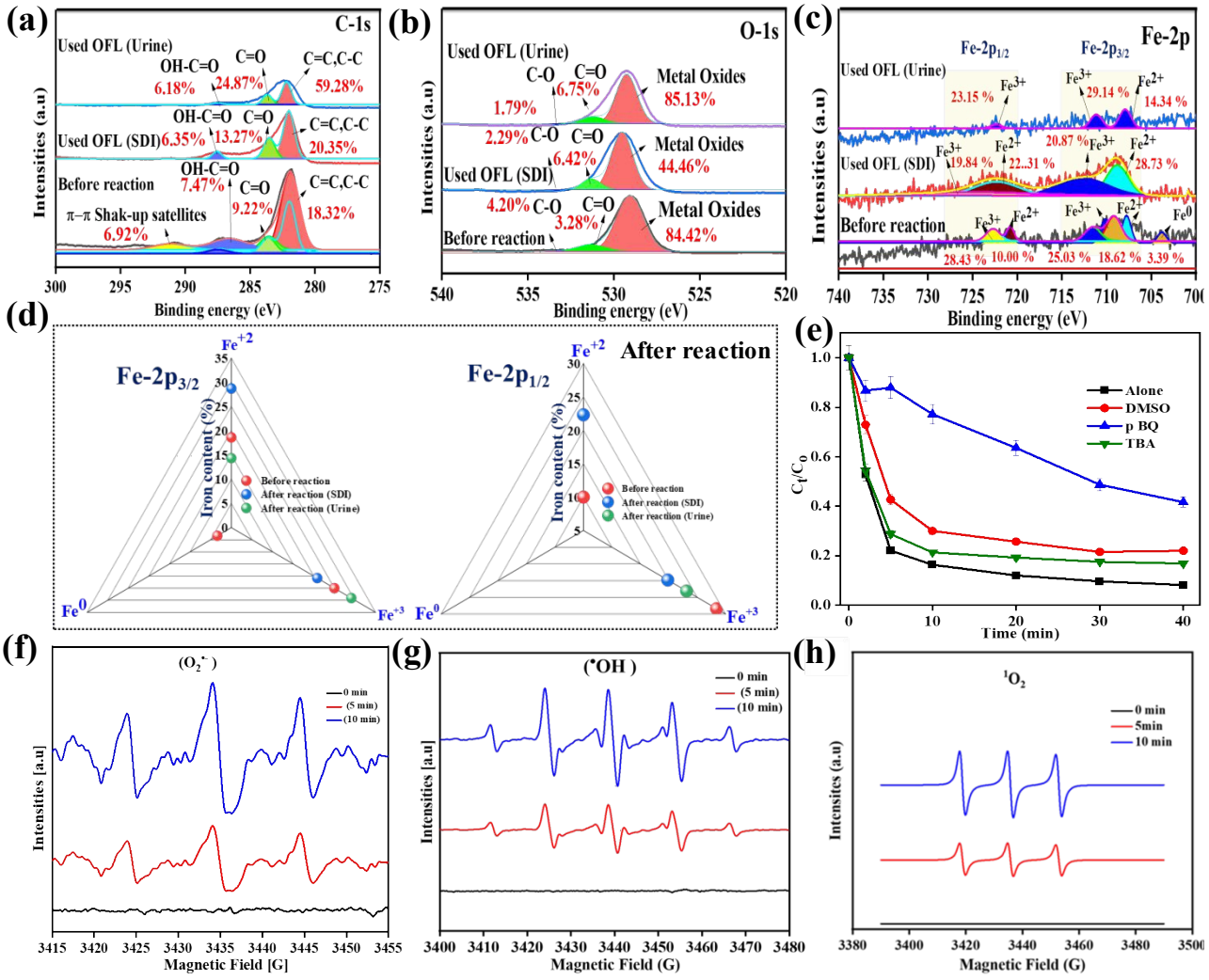

Figure 5: XPS of Fe-SCS@BR-700℃ before and after reaction under SID and stimulated urine (a) C-1s, (b) O-1s, and (c) Fe-2p (d) Iron contents changes (%). Scavenger tests of OFL stimulated urine (c)

View Article Online
DOI: 10.1039/D5EM00229A

and (f-h) EPR peaks under urine environment (OFL) over Fe-SCS@BR-700℃/O_3. **Conditions**: [OFL] = 20 mg/L, [V] = 200 mL, [O_3] = 5.5± 0.5 mg/L, catalyst = 0.2 g, pH (stimulated urine) = 9.17, scavengers' concentration = 0.2 mM, T =25℃ ±0.5℃, Time = 40 min, revolutions = 650 rpm

Based on previous results and after reaction, XPS analysis, a comprehensive degradation mechanism was proposed. Oxygen-containing functional groups played a crucial role as active sites for ROS production in decomposing O_3 in carbon-based material. **Figure 5 (a-c)** depicts the XPS peaks change before and after the catalyst reaction. **Figure 5 (a)** shows a reduction of the C-1s pattern after the reaction C=C (Alkane), C-C (covalent bond) from 18.32% to 20.35%, 59.28%, and 52.15% SDI water and stimulated urine, respectively. While the enhancement of the carbonyl group (C=O) was noticed. C=C and C-C acted as π-electron donors while OH-C=O and π-π electron variations were observed, indicating a successful reaction. **Figure. 5b** shows that metal oxide (Fe_2O_3, Fe_3O_4, $CaCO_3$, SiO_2, and Calcite) has played a significant role, and the C-C plays a donor role by enhancing C=O. Before the reaction, **Figure. 6c** depicts the distinct peaks of Fe-2p (Fe-$2p_{2/3}$ to Fe-$2p_{1/2}$) before and after reaction. Notably, Fe^0 (3.39%) was formed due to the conversion of Fe_2O_3 and Fe_3O_4 at an enhanced carbothermal temperature [41], already confirmed by XRD and FTIR **(Figure 5 (a, b)).** Moreover, before the reaction, peaks of Fe-$2p_{3/2}$ were divided into Fe^{+2} (707.7 eV) (18.62%) and Fe^{+3} (710.3 eV) (25.03%), while Fe-$2p_{1/2}$ were divided into Fe^{+2} (721.7 eV) (10.0%), Fe^{+3} (722.9 eV) (28.43%). After reaction, significantly distinct changes into peaks were seen in both water matrices **(Figure 5d).** In SDI water, Fe-$2p_{3/2}$ (Fe^{+2} and Fe^{+3}) peaks were changed from 18.62% and 25.03% to 28.73% and 20.87%, respectively. While in urine, Fe^{+2} (14.34%) and Fe^{+3} (29.14%) peak changes were observed. Interestingly, Fe^0 has acted as an electron donor, confirmed by EIS **(Figure 2e)**, and facilitated a redox reaction to generate ROS. Finally, these novel mechanistic insights revealed that

View Article Online
DOI: 10.1039/D5GC04029A

iron-rich nano-composites like SCS@BR-700℃ can dominate redox reactions in a real urine environment. Notably, these findings align with experimental results **(Figure 3a, b),** which means these breakthrough results unlock potential for real-world antibiotic (e.g., OFL) remediation in challenging waste streams.

Scavenger experiments **(Figure 5e)** were performed in the Fe-SCS@BR-700℃/O_3 system under urine to determine the O_3 activation to ROS generation. Tert-butyl alcohol (TBA) indicated the $^{\bullet}OH$ ($k_{\bullet OH\ TBA}$ = (3.8–7.6) × 10^8 $M^{-1}\cdot s^{-1}$) while Benzoquinone (BQ) trapped the $O_2^{\bullet-}$ ($k_{O2\bullet-\ BQ}$ = 1.0 × 10^9 $M^{-1}.\ s^{-1}$) [40]. Importantly, DMSO (5,5-dimethyl-1-pyrroline N-oxide) scavenged the $O_2^{\bullet-}$, $^{\bullet}OH$ and $^1O_2$. **Figure. 5e** confirmed that all ROS hindered the reaction, and scavenging of $O_2^{\bullet-}$ (OFL = 58.34%) showed a serious impact during the degradation under urine. Hence, $O_2^{\bullet-}$ confirmed a critical role in the Fe-SCS@BR-700℃/O_3 system containing OFL in stimulated urine. To investigate the ROS, an EPR spin-trapping was performed under stimulated urine, after 5-10 min, to detect the presence of ROS using DMPO and TMEPO. **Figure.5 (f-g)**, distinct strong signals of $O_2^{\bullet-}$, and $^{\bullet}OH$ were noticed relatively. However, limited signals of $^1O_2$ **(Figure h)** have significant removal (83.12%) over the TBA scavenging, while $O_2^{\bullet-}$ signals already proved relatively strong and tolerant in the urine environment. Interestingly, the above-mentioned mechanism has revealed the electron donor and redox reaction ability of Fe-$2p_{3/2}$, Fe-$2p_{1/2}$, and $Fe^{0,}$ which played a vital role in ROS generation.

5. Catalytic degradation mechanism verified by DFT calculations

To elucidate the above-mentioned ROS and active sites results, a DFT study was performed to reveal adsorption-promoted synergies between O_3 and SCS's Fe content over various functional groups' active sites for OFL degradation. **Figure S5c** depicts the FMO of the raw BR and Fe-

View Article Online
DOI: 10.1039/D5GC04029A

SCS@BR-700℃ after co-pyrolysis, confirming electron transfer ability.

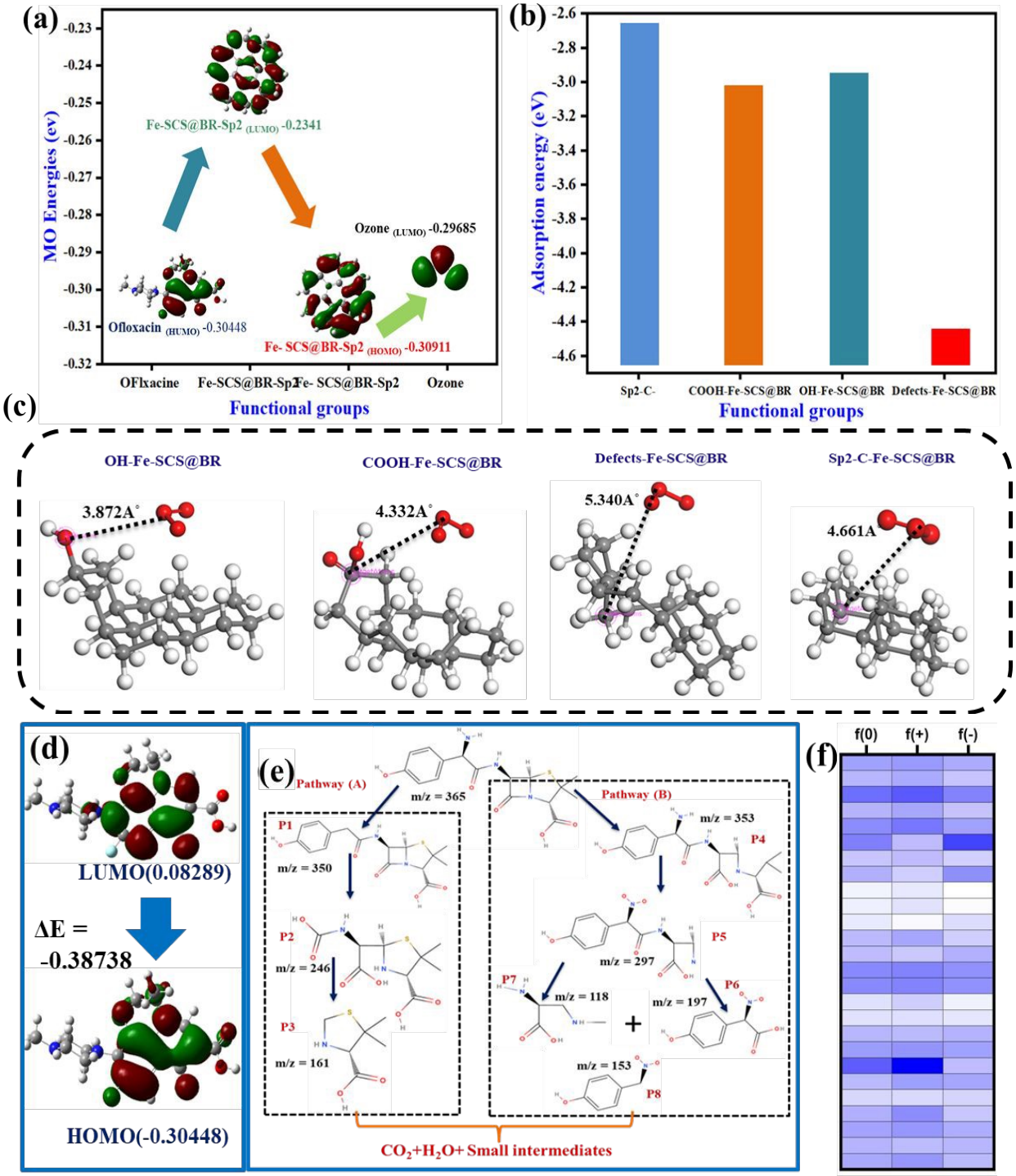

Figure 6: (a-b) Direct ozonation (FMO structures of the raw Fe-SCS@BR after co-pyrolysis and ozone role for electron transfer for OFL) (c) Adsorption energies and (d) Adsorption distance of ozone over different models of Fe-SCS@BR-700℃, (d) HUMO and LUMO of OFL (easily degradation sites) (e) Degradation pathway of Amoxicillin (recalcitrance then other antibiotics) under urine environment, over Fe-SCS@BR-700℃/O3, (f) AMO Fukui indices.

View Article Online
DOI: 10.1039/D5GC04029A

Figure 6a depicts that the sp^2-hybridized over Fe-SCS@BR-700℃ could transform delocalized π electrons. This could transfer from the LUMO (-0.2341 eV) of the sp^2-hybridized orbital to its HOMO (-0.30911 eV) orbital due to the HOMO-LUMO gap. Finally, direct ozonation could occur between Ofloxacin and O_3 [42]. **Figure 6c** shows DFT calculations for different adsorption values of Fe-SCS@BR-700℃ over O_3. All adsorption models were established based on Fe-SCS@BR-700℃'s XPS and FTIR results. Optimization was performed using the Forcite model to calculate energies, and further adsorption locator models having an initial adsorption distance of 10 A˚ were applied to estimate the total energy of the particular adsorption model separately. As per the following **Equation, 3** different models of Fe-SCS@BR-700℃/O_3 (Ozone E_{ads} = 42.38 kcal/mol) were calculated (**Table S3).**

$$E_{ads}=E_{adsorption\ system}-E_{catalyst}-E_{O_3} \qquad (3)$$

All adsorption energies and distances of the O_3 over the SCS@BR-700℃'s surface functional groups are shown in **Table S3**. Adsorption energy varies from -2.75 eV to -4.50 eV, which means strong adsorption of O_3 over Fe-SCS@BR-700℃ is due to exothermic interactions. This means that the highest adsorption energy of O_3 over defects-Fe-SCS@BR-700℃ was -4.50 eV, while having the longest adsorption distances at 5.340 A˚. It is demonstrated that interaction at defect sites allows for an adsorption over a longer distance while still maintaining a strong interaction [43]. **Figure 6d** confirmed the possibly different adsorption distances, confirming the adsorption of O_3 over different Fe-SCS@BR-700℃ models during reaction.

6. DFT calculations, possible degradation pathways

Fukui function and DFT calculations were performed to investigate the vulnerable reactive sites

View Article Online
DOI: 10.1039/D5GC04029A

revealed by HUMO and LUMO of the OFL that possibly caused degradation over Fe-SCS@BR-700℃/O_3, **Figure 6 (e-i)** and **Figure S6.** OFL's Fukui indices are shown in **Figure 6 (i-j)** and the **Table. (S4-S6).** It is already documented that atoms with higher values of f^0 are more susceptible to ROS [44]. It was seen that OFL has O3, O5, N6, C14, and C20 as more susceptible atoms to be attacked by ROS, as shown by color clouds **(Figure 6 i-j).** For OFL, possible degradation pathways investigation, samples were collected over Fe-SCS@BR-700℃/O_3 and filtered using a 45-μm filter at a particular time. Later, Liquid Chromatography-Mass Spectrometry (LC-MS) was performed to reveal the intermediates **Figure S9.**

Figure 6 (g) proposed possible OFL degradation pathways based on DFT and identified intermediates. In **Pathway (A)**, P1 (m/z = 350) was formed due to higher f^0 N9 values (0.068) **(Table S4),** which $O_2^{\bullet-}$ could attack and $^1O_2$. While the C=O group was broken near the benzene and β-lactam rings to generate P2 (m/z = 246) [45]. Besides the limited $^{\bullet}OH$ **(Fig. 6 (a-b)),** it could still cause the conversion of P2 (m/z = 246) to convert into intermediates P3 (m/z = 161), finally reaching mineralization of intermediates to CO_2 and H_2O and small intermediates. **Pathway (B)** depicts the OFL degradation pathways by the cleavage of the amide bond and the decarboxylation reaction. OFL's S1**,** with higher values of f^0 (0.048) **(Table S4-S6),** was susceptible to free radicals like $O_2^{\bullet-}$ and $^1O_2$. Later, **P4** to **P5** intermediates could be converted due to the attack of ROS by O_3 over Fe-SCS@BR-700℃ on the benzene group, and oxidation of the phenolic hydroxyl group. Further, under the combined attack of $^{\bullet}OH$, $O_2^{\bullet-}$, and $^1O_2$, decarboxylation, amide bond oxidation, and amino group oxidation will move towards CO_2 and H_2O and small intermediates [45].

View Article Online
DOI: 10.1039/D5GC04029A

7. Proposed reaction mechanism

Based on the investigation of Fe-SCS@BR-700℃/O_3's degradation active sites change, before and after reaction, revealed by XPS, a possible reaction mechanism of OFL in the urine was proposed **(Scheme 1)**. Heterogeneous catalytic ozonation degradation of organic compounds has several pathways to decompose the O_3 [46]. The strong appearance of superoxide $O_2^{\bullet-}$, $^1O_2$, and $^{\bullet}OH$ has been detected by scavengers and EPR tests. Organic urine substances like creatine, creatinine, and hippuric acid can hinder the catalytic reaction due to scavenging effects **(Figure 4 (d-e))** [27]. Based on the DFT adsorption study of O_3 over the Fe-SCS@BR-700℃ surface (**Figure 6d**), defects in the structure are directly responsible for oxygen-rich species generation, due to enhanced electron transfer [47]. O_3 activation could be determined by the free-flow π-electron produced by sp^3 carbon-abundant material[48] **(equation 4-9).**

$$\text{Carbon-}\pi + 2H_2O \rightarrow \text{Carbon-}H_3O^+ + {}^{\bullet}OH \quad (4)$$

$$O_3 + OH \rightarrow {}^{\bullet}HO_2 + O_2^{\bullet-} \quad (5)$$

$${}^{\bullet}HO_2 \rightarrow O_2^{\bullet-} + H^+ \quad (6)$$

OR

$$O_3 + H_2O \rightarrow 2\,{}^{\bullet}OH + O_2 \quad (7)$$

$$O_3 + OH^- \rightarrow O_2^- + HO_2^- \quad (8)$$

$$O_3 + {}^{\bullet}OH \rightarrow O_2 + HO_2^{\bullet} \leftrightarrow O_2^{\bullet-} + H^+ \quad (9)$$

Based on XPS spectra before and after the reaction, it was investigated that oxygen-containing functional groups like C=O, $^{\bullet}OH$, and COOH, and sp^2-hybridized orbital or metal ions like Fe^0, Fe^{+2}, or Fe^{+3} **(Figure 7)** could enhance the O_3 depletion and ROS generation like $^{\bullet}OH$, $^1O_2$, and $O_2^{\bullet-}$ over

View Article Online
DOI: 10.1039/D5GC04029A

Fe-SCS@BR-700°C [49]. **(i)** As per **equation 1-2,** the presence of Fe^0 ions in the Fe-SCS@BR-700°C is due to iron oxides at higher temperatures with carbon substances. **(ii)** Which can generate Fe^{+3} and Fe^{+2} **(equation 10-12),** trivalent iron species like Fe^{+3} can directly react with soluble O_3 and can donate free electrons towards O_3, resulting in $O_2^{\bullet-}$, $^1O_2$ and $^{\bullet}OH$ **(equation 5-6)** [49]**.** Meanwhile, $O_2^{\bullet-}$ could react directly with Fe^{+3}, generating $^1O_2$.

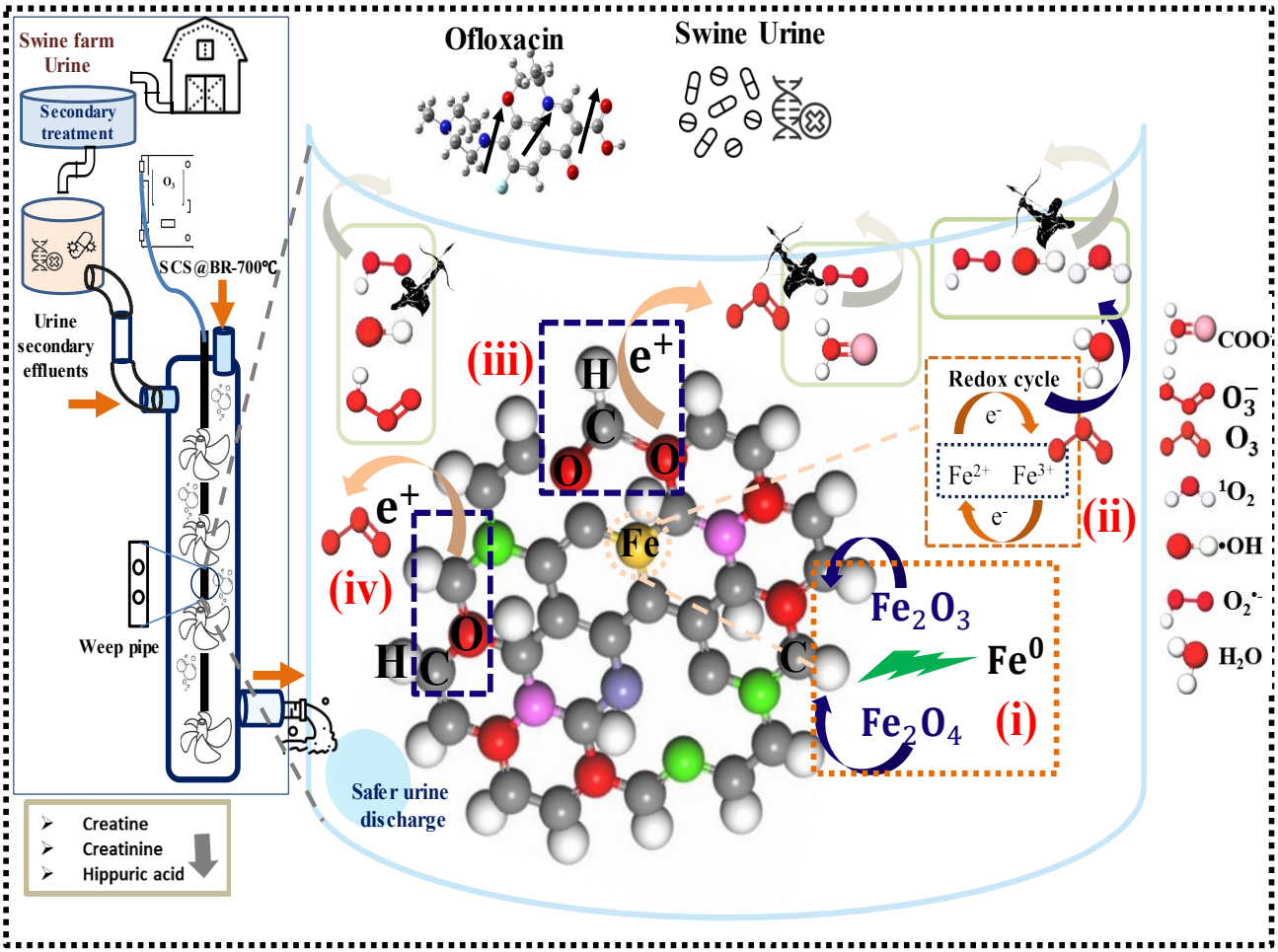

Scheme 01: Mechanistic illustration of the catalytic ozonation of OFL and real swine urine's pharmaceuticals degradation over the Fe-SCS@BR-700°C/O_3 system.

Moreover, the standard reduction potential (E_0) (Fe^{+2}/Fe^{+3}) = 0.77 V lower than O_3 (E_0 (O_3/ O_2)) = 2.07 V [50]. Therefore, O_3 will be split into ROS due to the iron species and could ultimately react

View Article Online
DOI: 10.1039/D5GC04029A

with the OFL, resulting in CO_2 and water.

$$\equiv Fe^{0}+2Fe^{+3}\rightarrow 3Fe^{+2} \quad (10)$$

$$\equiv Fe^{+3}+O_2^{\cdot-}\rightarrow Fe^{+2}+H^{+}+{}^{1}O_2 \quad (11)$$

$$\equiv Fe^{+3}+O_3+H_2O \rightarrow Fe^{+2}+2OH+O_2^{\cdot-} \quad (12)$$

(iii) It is documented that oxygen-rich species of abundant material like COOH could donate electrons to O_3, resulting in $^{\bullet}O_3^{-}$, $^{\bullet}OH$, and $O_2^{\bullet-}$ **(Equation 13).**

$$3COOH + 2O_3 \rightarrow 3COO^{\bullet} + 3O_2^{\bullet-} + 3H^{+} \quad (13)$$

(iv) Further, another C=OH group could donate free electrons to O_3, resulting $O_2^{\bullet-}$, $O_3^{\bullet-}$ and $^{\bullet}OH$. **(Equation 14)**

$$C{=}OH + O_3 \rightarrow O_3^{\cdot-} + C{=}O^{\cdot} + H^{+} \quad (14)$$

As per results, Fe-SCS@BR-700℃/O_3 degradation **(Figure 3a-b)** was higher than single ozonation due to abundant ROS. Hence, DFT revealed the possible adsorption of O_3 over Fe-SCS@BR-700℃'s surface groups to produce ROS, confirmed by scavenger test, EPR, and XPS results before and after reaction. Consequently, Fe-SCS@BR-700℃ has successfully activated the O_3 for the ROS generation, possibly involved in catalytic ozonation degradation of OFL into smaller intermediates, CO_2, and H_2O**.** Further, a vertical economic fixed-bed design for adsorption support ozonation for small pigsties was proposed for better mixing and efficiency.

8. Environmental implications and evaluation assessment

8.1 Biological toxicity and LCA assessment over Fe-SCS@BR@700℃

Evaluating the heavy metal leaching for steel convert slag-based catalysts like Fe-SCS@BR-700℃ should be a primary concern for biological toxicity and impact assessment. To determine the

View Article Online
DOI: 10.1039/D5GC04029A

safer optimum catalytic dose of the Fe-SCS@BR-700℃ against OFL solution, various dosages of 0.1 g, 0.2 g, and 0.3 g were tested **(Figure 7a)**.

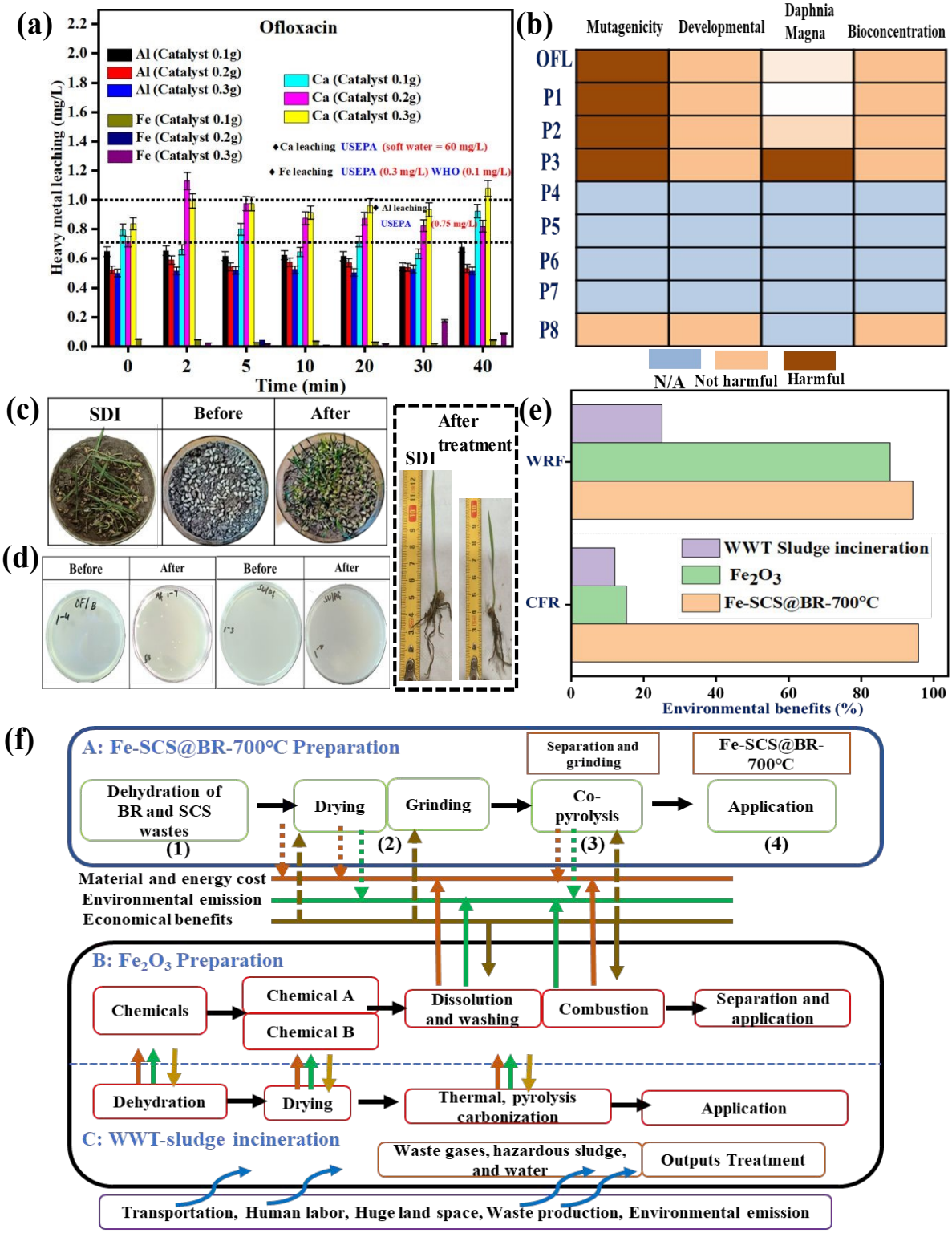

Figure 7: Optimum Fe-SCS@BR-700℃/O_3 dosage (a) heavy metal leaching, (b) Toxicity assessment,

(c) Wheat grain growth under ozonated urine and SDI. (d) Escherichia coli (E. coli) growth experiment under OFL and swine urine (e) Environmental benefits (f) System boundaries for waste-based Fe-SCS@BR-700℃, chemically synthesized Fe_2O_3, and sludge disposal. **Conditions**: [OFL] = 20 mg/L, [V] = 200 mL, [O_3] = 5.5± 0.5 mg/L, catalyst = (0.1-0.3) g, pH (urine) = 8.85, pH (stimulated) = 9.17, T =25℃ ± 0.5℃, Time = 100 min, revolutions = 650 rpm, (c, d) **Text.S6. (details)**.

Later samples were collected for the ICP-MS. Most abundant toxic metals leaching over the catalyst to the solution, like Al, Fe, and Ca, were evaluated against the World Health Organization (WHO) and United States Environmental Protection Agency (USEPA) standards for drinking water. It was seen that Fe and Al leaching were 0.1 mg/L-0.3mg/L, and 0.75 mg/L, respectively, under the safer limit per WHO and USEPA guidelines for aquatic life and ambient water quality. Notably, Ca leaching was in favor of the aquatic ecological environment. Finally, based on metal leaching results, 0.1g-0.2g of the catalysts were considered environmentally benign. Consequently, the biological toxicity assessment of the treated OFL solution and ozonated urine's intermediates was practically investigated by germinating wheat seeds **(Figure 7c)**. Based on observations, germination under real soil conditions, where 95.5% occurred within 5 days, was irrigated by SDI water. No growth was observed due to the OFL contamination. However, after treatment over Fe-SCS@BR-700℃/O_3, significant recovery (85.5%) of the grain's growth was observed under soil conditions. It was observed that the biological toxicity after treatment was significantly reduced. Additionally, Escherichia coli (E. coli) growth by petri plate experiments, over OFL, and swine urine before and after catalytic ozonation degradation was performed over 12 hr. **(Text S6).** As per analysis **(Figure 7d),** it was seen that E. coli growth was inhibited before the reaction due to the presence of antibiotics or organic pollutants, but after the reaction, significant growth was observed. Finally, swine urine's organic pollutants were

View Article Online
DOI: 10.1039/D5GC04029A

successfully eliminated over Fe-SCS@BR-700℃/O_3. Notably, Fe-SCS@BR-700℃ has also satisfactorily performed under real water conditions **(Figure S13b).** Moreover, ozonated urine successfully meets the international organizations' water quality standards parameters **(Figure S14).** Hence, the novel nano-composite proved greener and multi-functional for the degradation of OFL and real swine urine complex matrix **(Figure 7e).**

To meet the carbon dioxide emissions reduction by 2030 and achieve carbon neutrality by 2060, as announced by the 75th UN General Assembly in 2020, a potential solution has been proposed by Fe-SCS@BR-700℃, with life cycle assessment analysis (LCA) **(Figure 7e-f) (Text S7)**. To evaluate all possible environmental, economic, and social benefits, studies were performed **(Table S9-11)**. Although the analysis's data is not perfect, it can be easily concluded that the synthesis waste-based Fe-SCS@BR-700℃ catalyst has significant environmental and economic benefits compared to chemically synthesized Fe_2O_3 and sludge incineration. Based on results, 1 ton of Fe-SCS@BR-700℃ costs 220$, while only 0.4 tons of Fe_2O_3 costs 920$. Finally, it was seen that waste-based catalysts not only address the waste reduction factor (WRF) and carbon footprint reduction (CFR) comparatively **(Figure 7e),** but also reduce the cost associated with sludge incineration and disposal. Finally, the synthesizing catalysts by a combination of organic wastes and exogenous metals from industrial metal residues could be extended to various industrial and agricultural wastes, to reveal the real potential for upcycling of hazardous wastes for practical environmental remediation. Further to calculations, CO_2 equivalents avoided by waste-based Fe-SCS@BR-700℃ catalyst, comprehensive calculations were performed as per standard methods in **TextS7 (1-5) (i), (ii), (iii),** and comprehensive analysis results were mentioned in the **Table S12 (i), (ii), (iii).** Finally, it was concluded that Fe-SCS@BR-700℃

View Article Online
DOI: 10.1039/D5GC04029A

achieves a net carbon saving of over 16,000 kg CO_2 per 0.4 kg batch, resulting in a 222.1 carbon savings ratio, which means every 1 kg of carbon invested saves 222 kg of emissions. It's a tremendously effective way to reduce emissions. These advantages demonstrate the Fe-SCS@BR700℃ catalyst's strong potential for real-world adoption

8.2 Performance comparison, safer disposal, and installation cost

Fe-SCS@BR-700℃ catalyst satisfactorily performed while comparing commercially available catalysts like Fe_2O_3, Fe_3O_4, MnO_2, and TiO_2 or other waste-based catalysts **(Figure S13a, Table S15b).** Importantly, safer disposal of the utilized Fe-SCS@BR-700℃, washing the catalyst with a polar solvent like ethanol, was recommended to extract organic pollutants [34]. Sodium silicate (Na_2SiO_3) was also recommended to reduce the heavy metal leaching risk [35]. These steps could effectively stop the heavy metal leaching risk and antibiotic introduction by the used catalyst. Importantly, installation of an adsorption-assisted, catalytic, efficient ozonation degradation system powered by solar energy offers a cost-effective solution for swine urine treatment at small and medium-scale pig farms. Fe-SCS@BR-700℃ catalyst is prepared in a lab at an estimated cost of 0.0725 $/g. For 400 L of urine (200 pigs), 300g of Fe-SCS@BR-700℃ will be utilized daily. Further comprehensive estimated system installation cost analysis and cost comparison for the proposed system are shown in **Table S13a-b.** Additionally, **Table S14 a-c** depicts the catalyst preparation cost based on efficiencies, stability comparison with other catalysts/technologies. Additionally, E-factors and real swine urine treatment comprehensive comparison was performed **(Table S15a-b)**. Finally, it was concluded that this proposed system combines low costs, high efficiency, and environmental benefits, making it ideal for small and medium-sized industrial applications.

View Article Online
DOI: 10.1039/D5GC04029A

9. Conclusion

In summary, this study presents novel and economical Fe-SCS@BR-700℃ nano-composite as an efficient catalyst that was thoroughly investigated and successfully prepared by one-pot co-pyrolysis of BR and SCS. By leveraging the unique synergistic integration at higher temperatures (i.e., 700℃) revealed by characterizations, like uniform iron species, excellent acceleration of O_3 decomposition, and electron transfer, optimum ROS generation was obtained. Further, the combined effect of adsorption-enhanced efficient ozonation, Fe-SCS@BR-700℃, had not only significantly degraded OFL in stimulated urine, but also eliminated the organic pollutants from real swine urine, including various toxic antibiotics under different experimental settings. Enhanced degradation of real swine urine was confirmed by COD and TOC, and 3D-EEM for a small pigsty. Meanwhile, $O_2^{\bullet-}$ showed a significant role compared to $^{\bullet}OH$, $^1O_2$, confirmed by scavenging and EPR results. Similarly, a DFT study has verified the Fe-SCS@BR-700℃'s active sites for the direction and indirect of ozonation via electron transfer and OFL's vulnerable attacking sites by ROS, like $O_2^{\bullet-}$. Finally, the proposed mechanism revealed a unique synergy for O_3 decomposition, an abundance of active sites (Fe^0, Fe^{+2}, or Fe^{+3}), and mass transfer due to adsorption-promoted enhanced ozonation. Moreover, safer catalytic dosage for effluent and after reaction usage for practical environmental applications like wheat grain and E. coli growth in real conditions was successfully investigated. Furthermore, performance assessments and cost analyses indicate that the technology offers unprecedented dual benefits, offering a promising and sustainable green solution for small pigsties to significantly remove urine's pharmaceuticals, to meet national livestock wastewater discharge regulations. This could be an effective economic strategy to utilize hazardous industrial wastes in the real environment, like fresh

View Article Online
DOI: 10.1039/D5GC04029A

waters, and resource utilization.

Abbreviations:

Biogas residue (BR), Steel converter slag (SCS), Energy-dispersive X-ray spectroscopy (EDX), Fourier transform infrared spectrometer (FTIR), Superoxide radical ($O_2^{\bullet-}$), Singlet oxygen ($^1O_2$), Hydroxyl Radical ($^{\bullet}OH$), Para-benzoquinone (PBQ), Reactive oxygen species (ROS), Scanning electron microscope (SEM), Tert-butyl-alcohol (TBA), X-ray photoelectron spectroscopy (XPS), X-ray diffraction (XRD), X-ray fluorescence (XRF), Amoxicillin (AMO), Ofloxacin (OFL), Oxytetracycline (OTC), Norfloxacin (NOR), Sulfa-methazole (SMZ), Mebendazole (MBZ), Sulfacetamide (SM), Doxycycline hydrochloride (DOC), Sulfamonomethoxine (SMX), Sulfacetamide (SM), High-Performance Liquid Chromatography (HPLC), Triple Quadrupole Liquid Chromatography-Mass Spectrometry (QTRAP ABI-3200), LC-MS (Liquid Chromatography-Mass Spectrometry), Inductively Coupled Plasma Mass Spectrometry (ICP-MS), Life cycle assessment (LCA), Waste reduction factor (WRF), Carbon footprint reduction (CFR).

Funding

This work was supported by the Science and Technology Project of Fujian Province (2023T3011), the Collaborative Innovation Platform Program of Fu-Xia-Quan National Innovation Demonstration Zone (3502ZCQXT2022004), and the Youth Science and Technology Innovation Program of Xiamen Ocean and Fisheries Development Special Funds (23YYST061QCA09)

View Article Online
DOI: 10.1039/D5GC04029A

10. References.

1. L. Hao, J. Yan, J. Guo, N. Wang and M. Zeng, *Journal of Environmental Chemical Engineering*, 2025, **13**, 115546.
2. T. P. Van Boeckel, J. Pires, R. Silvester, C. Zhao, J. Song, N. G. Criscuolo, M. Gilbert, S. Bonhoeffer and R. Laxminarayan, *Science*, 2019, **365**, eaaw1944.
3. H. Bao, Z. Chen, Q. Wen, Y. Wu and Q. Fu, *Bioresource Technology*, 2024, **393**, 130127.
4. K. Zhang, R. Ruan, Z. Zhang and S. Zhi, *Science of The Total Environment*, 2022, **847**, 157688.
5. Y. Yu, N. Jiang, Y. Zhou, F. Huang, Y. He and Y. Zhang, *Journal of Environmental Management*, 2025, **373**, 123960.
6. B. Li and T. Zhang, *Water Research*, 2012, **46**, 3703-3713.
7. K.-F. Yu, P. Li, H. Li, B. Zhang, J. Yang, F.-Y. Huang, R. Li and Y. He, *Journal of Hazardous Materials*, 2021, **406**, 124295.
8. C. Liang, D. Wei, S. Zhang, Q. Ren, J. Shi and L. Liu, *Ecotoxicology and Environmental Safety*, 2021, **210**, 111885.
9. J. Wang, Z. Yu, T. Zhao, Y. Song, H. Liu, J. Hou and P. Yu, *Applied Surface Science*, 2025, **709**, 163837.
10. B. Chen, Y. Zhu, M. Wu, Y. Xiao, J. Huang, C. Lin and B. Weng, *Journal*, 2024, **16**.
11. A. Reza and L. Chen, *Environmental Chemistry Letters*, 2022, **20**, 1863-1895.
12. H. Wu and C. Vaneeckhaute, *Chemical Engineering Journal*, 2022, **433**, 133664.
13. B. B. Garcia, G. Lourinho, P. Romano and P. S. D. Brito, *Heliyon*, 2020, **6**, e03293.
14. J. Liu, X. Bai and Y. Bai, *Water Cycle*, 2024, **5**, 278-285.
15. H. Kong, K. Luo and Z. Yong, *Waste Management*, 2024, **180**, 36-46.
16. M. Stefaniuk and P. Oleszczuk, *Journal of Analytical and Applied Pyrolysis*, 2015, **115**, 157-165.
17. Y. Wang, G. Yu, S. Xie, R. Jiang, C. Li and Z. Xing, *Fuel*, 2023, **353**, 129185.
18. G. P. Muthukutti, M. K. Singh, S. K. Palaniappan, K. Vijayananth, S. M. Rangappa and S. Siengchin, *Chemical Engineering Journal*, 2025, **512**, 162344.
19. W. Xu, S. Dong, H. Cheng, S. Giannakis, X. Lu, Z. He, D. Wang, S. Song and J. Ma, *Chemical Engineering Journal*, 2025, **513**, 162624.
20. L. Li, Y. Hua, S. Zhao, D. Yang, S. Chen, Q. Song, J. Gao and X. Dai, *ACS ES&T Engineering*, 2023, **3**, 1083-1097.
21. K. Xu, Q. Lin, X. Fan, J. Zheng, Y. Liu, Y. Ma and J. He, *Chemical Engineering Journal*, 2023, **460**, 141578.
22. Y. Wang, X. Liu, Z. Cao, W. Zhang and Y. Xue, *Materials Letters*, 2021, **304**, 130734.
23. J. Li, L. Pan, G. Yu, S. Xie, C. Li, D. Lai, Z. Li, F. You and Y. Wang, *Science of The Total Environment*, 2019, **654**, 1284-1292.
24. T. Jiang, B. Wang, M. Hassan and Q. Zou, *Carbon Research*, 2024, **3**, 78.
25. X. Li, H. Liu, Y. Zhang, J. Mahlknecht and C. Wang, *Journal of Environmental Management*, 2024, **352**, 120051.

View Article Online
DOI: 10.1039/D5GC04029A

26. R. Sun, R. Huang, J. Yang and C. Wang, *Chemosphere*, 2021, **285**, 131560.
27. X. Kang, L. Wang, J. Song and Q. Zhang, *Chemical Engineering Journal*, 2024, **493**, 152588.
28. Q. Yu, G. Liu, J. Shi, T. wen and L. Li, *Journal of Environmental Chemical Engineering*, 2022, **10**, 108553.
29. C. Fang, L. Nie, H. Chen and Y. Yang, *Journal of Water Process Engineering*, 2024, **63**, 105434.
30. V. Benavente, S. Lage, F. G. Gentili and S. Jansson, *Chemical Engineering Journal*, 2022, **428**, 129559.
31. A. Srikhaow, C. Chuaicham, J. Trakulmututa, K. Shu and K. Sasaki, *Sustainable Energy & Fuels*, 2024, **8**, 3065-3076.
32. X. Li, J. Lan, Y. Zhang, P. Chen, S. Ding, M. Nie and S. Li, *Journal*, 2025, **18**.
33. P. Zhang, W. Wei, Y. Shang and B.-C. Ye, *Bioresource Technology*, 2023, **385**, 129421.
34. K. Wang, C. He, S. You, W. Liu, W. Wang, R. Zhang, H. Qi and N. Ren, *Journal of Hazardous Materials*, 2015, **300**, 745-753.
35. E. Baumgarten, M. Nagel and R. Tischner, *Applied Microbiology and Biotechnology*, 1999, **52**, 281-284.
36. R. Yuan, Y. Qin, C. He, Z. Wang, L. Bai, H. Zhao, Z. Jiang, L. Meng and X. He, *Arabian Journal of Chemistry*, 2023, **16**, 104415.
37. A. Behnami, J.-P. Croué, E. Aghayani and M. Pourakbar, *RSC Advances*, 2021, **11**, 36965-36977.
38. J. Sun, H. Wu, C. Fu, C. Zhang, Z. Hu and M. Zhou, *Applied Catalysis B: Environment and Energy*, 2024, **351**, 123976.
39. E. Issaka, J. N.-O. Amu-Darko, S. Yakubu, F. O. Fapohunda, N. Ali and M. Bilal, *Chemosphere*, 2022, **289**, 133208.
40. M. Noman, G. Yu, D. Tsegaye Awugichew and X. Li, *Environmental Research*, 2024, **257**, 119314.
41. X. Sun, X. Ni, X. Wang and D. Xu, *Surfaces and Interfaces*, 2022, **31**, 102053.
42. Y. Cheng, B. Wang, P. Yan, J. Shen, J. Kang, S. Zhao, X. Zhu, L. Shen, S. Wang, Y. Shen and Z. Chen, *Chemical Engineering Journal*, 2023, **454**, 140232.
43. S. Mallikarjun Sharada, R. K. B. Karlsson, Y. Maimaiti, J. Voss and T. Bligaard, *Physical Review B*, 2019, **100**, 035439.
44. S. Yang, X. Liu, S. He, C. Jia and H. Zhong, *Journal of Molecular Liquids*, 2024, **394**, 123688.
45. D. Zhang, Y. Liu, Y. Song, X. Sun, W. Liu, J. Duan and Z. Cai, *Separation and Purification Technology*, 2023, **313**, 123430.
46. V.-R. Le, T.-B. Nguyen, C.-W. Chen, C. P. Huang, X.-T. Bui and C.-D. Dong, *Separation and Purification Technology*, 2023, **315**, 123672.
47. Y. Yang, Y. Chi, K. Yang, Z. Zhang, P. Gu, X. Ren, X. Wang, H. Miao and X. Xu, *Journal of Colloid and Interface Science*, 2023, **652**, 350-361.
48. M. Noman, G. Yu, E. A. Elimian and K. Yun, *Journal of Environmental Chemical Engineering*, 2025, **13**, 115236.
49. J. Zhang, L. Yang, C. Liu, J. Ma, C. Yan, S. Mu and M. Yu, *Separation and Purification Technology*, 2024, **340**, 126767.

50. J. Wang, Z. Huang, W. Liu, C. Chang, H. Tang, Z. Li, W. Chen, C. Jia, T. Yao, S. Wei, Y. Wu and Y. Li, *Journal of the American Chemical Society*, 2017, **139**, 17281-17284.

The data that support the findings of this study are available upon reasonable request.

View Article Online
DOI: 10.1039/D5GC04029A